Tunability of acoustic spectral gaps and transmission in periodically stubbed waveguides

X. F. Wang,[1] M. S. Kushwaha,[2] and P. Vasilopoulos[1]
[1]*Department of Physics, Concordia University, 1455 de Maisonneuve Blvd. West, Montreal, Quebec, Canada H3G 1M8*
[2]*Institute of Physics, University of Puebla, P.O. Box J-45, Puebla 72570, Mexico*
(Received 22 June 2001; published 14 December 2001)

A theoretical investigation is made of acoustic wave propagation in a periodically stubbed waveguide. In general the waveguide segments and stubs are made of different materials. The acoustic wave in such a system has two independent polarizations: out-of-plane and in-plane modes. The band structure and transmission spectrum is studied for diverse geometries using a simple and efficient version of the transfer-matrix method. For the *same material* between the waveguide and *symmetric* stubs the width of some gaps can change, upon varying the stub length or width, by more than one order of magnitude. A further modulation can be achieved for *different material* between the stubs and the main waveguide or if the stubs are *asymmetric*. The gaps in the band structure of an infinitely long system correspond to those in the transmission spectrum of the same system but with *finite* number n of units. For n finite (i) there exist pseudogaps that gradually turn into complete gaps with increasing n and (ii) the introduction of defects gives rise to states in the gaps and leads to transmission resonances.

DOI: 10.1103/PhysRevB.65.035107 PACS number(s): 41.20.Jb, 42.25.Bs, 43.20.+g

I. INTRODUCTION

The term ''band-gap engineering'' is well known from decades of research in semiconductors. The recently discovered periodic dielectric structures, which exhibit a photonic band gap (PBG) analogous to the electronic band gap in semiconductors, have attracted considerable attention due to many interesting phenomena and potential applications emerging from them, such as the control of spontaneous emission of radiation, zero-threshold lasing, and the sharp bending of light.[1]

It did not take long before the study of PBG materials, involving light waves, led to analogous studies in other systems involving elastic/acoustic waves, e.g, the phononic crystals[2] or other periodic acoustic composites.[3] The phononic crystals[2] have drawn comparatively greater attention, both theoretically[4] and experimentally.[5,6] In analogy with PBG crystals, the emphasis in phononic crystals has been on the occurrence of complete acoustic gaps within which the sound, vibrations, and phonons are all forbidden. This is of interest for applications such as ultrasonic filters, noise control, and improvement in the design of transducers, as well as for fundamental physics concerned with the Anderson localization of sound and vibrations.[7]

The purpose of this paper is to study the acoustic band structure and transmission spectrum in a periodically modulated quasi-one-dimensional waveguide, as depicted in Fig. 1. The system has a finite (infinite) extension along the $y(z)$ direction and is periodically modulated, along the x direction, by the addition of double stubs, in general asymmetric, with different elastic properties than those of the main waveguide. The motivation stems from recent studies with interesting results pertinent to electronic[8] and photonic[9] waveguides modulated in the same fashion. Using the transfer-matrix technique we demonstrate the tunability of the acoustic band gaps as a function of various parameters of the system, e.g., the length and/or width of the stubs.

The rest of the paper is organized as follows. In Sec. II we introduce the formalism for studying the wave propagation in the allowed polarization and present the necessary details of the transfer-matrix method.[10] In Sec. III we present several illustrative numerical results on the band structure and transmission spectrum under various material and geometric conditions. The final section contains the concluding remarks.

II. FORMALISM

This section is divided into two parts. First we embark on the polarization pertinent to wave propagation in a two-dimensional (2D) system. Then we present the transfer-matrix method for quite a general geometry of the unit cell of acoustic stub tuners shown in Fig. 2.

A. Polarization of the wave

We start with the general equation of propagation of harmonic acoustic waves in an isotropic three-dimensional (3D) homogeneous medium

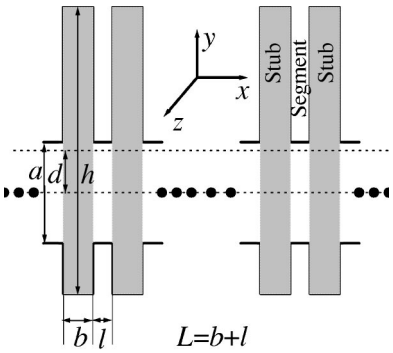

FIG. 1. Schematics of a quasi-one-dimensional periodic waveguide. The double stubs can be made of the same or different material than that of the main waveguide. $L=b+l$ is the period of the system.

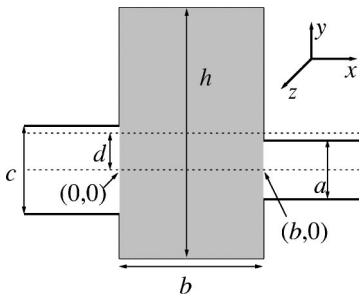

FIG. 2. Schematics of a general unit cell with asymmetric stubs.

$$(\lambda+\mu)\nabla(\nabla\cdot\mathbf{u})+\mu\nabla^2\mathbf{u}+\rho\omega^2\mathbf{u}=0, \tag{1}$$

where ρ is the mass density, ω the angular frequency, and λ and μ the Lame coefficients. The longitudinal v_l and transverse v_t speed of sound are defined in terms of the Lame coefficients $v_l=\sqrt{(\lambda+2\mu)/\rho}$ and $v_t=\sqrt{\mu/\rho}$. For a 2D system at hand the displacement vector $\mathbf{u}$ is independent of the z coordinate and one can take $\partial_z\equiv\partial/\partial z=0$. Then Eq. (1) can be written as

$$(\lambda+\mu)\nabla_p(\partial_x u_x+\partial_y u_y)+\mu\nabla_p^2(u_x\hat{i}+u_y\hat{j}+u_z\hat{k})$$
$$+\rho\omega^2(u_x\hat{i}+u_y\hat{j}+u_z\hat{k})=0, \tag{2}$$

where $\nabla_p=\hat{i}\partial_x+\hat{j}\partial_y$, and $\hat{i}$, $\hat{j}$, and $\hat{k}$ are the unit vectors along the x,y, and z axes, respectively. This equation is equivalent to the independent equations

$$(\nabla_p^2+k_t^2)u_z=0, \tag{3}$$

with $k_t=\omega/v_t$, and

$$(\lambda+\mu)\nabla_p(\nabla_p\cdot\mathbf{u}_p)+\mu\nabla_p^2\mathbf{u}_p+\rho\omega^2\mathbf{u}_p=0. \tag{4}$$

Here the subscript p is assigned to the quantities which qualify only in the x-y plane. It is thus quite reasonably understandable that a 2D system can support two independent modes: the *out-of-plane* modes and the *in-plane* modes, described, respectively, by Eqs. (3) and (4). Equation (4) can be further simplified as follows. We write

$$\mathbf{u}_p=\nabla_p\phi+\nabla_p\times\boldsymbol{\psi} \tag{5}$$

with $\boldsymbol{\psi}\equiv(0,0,\psi)$. Then Eq. (4) further splits into the equations

$$(\nabla_p^2+k_l^2)\phi=0, \tag{6}$$

with $k_l=\omega/v_l$, and

$$(\nabla_p^2+k_t^2)\psi=0. \tag{7}$$

Interestingly, Eq. (7), which describes the transverse in-plane vibrations, has formally the same structure as the one for the out-of-plane vibrations, Eq. (3). Also, Eqs. (3), (6), and (7) are formally identical to the scalar wave equation for the TE polarization in photonic crystals.[9]

It should be pointed out that the splitting of Eq. (4) into Eqs. (6) and (7), is valid only for a homogeneous medium. For an inhomogeneous medium, when λ and μ are functions of position, this is no longer possible.[11] If the system is piecewise homogeneous, as the one we consider in Sec. III B, problems arise in the application of the boundary conditions at the interface of different regions[12] that make the separation of the in-plane modes in pure longitudinal and transverse ones impossible.

B. Transfer-matrix technique

For the sake of generality, we start with a crossbarlike geometry of a single unit cell, as shown in Fig. 2. The origin of the Cartesian coordinates is at the uniaxial line intersecting perpendicularly the left arm of the stub of width b and length h. The center of the asymmetric stub lies at $(x=b/2,d)$. We denote the width of the left (right) waveguide segments by $c(a)$ and take the x axis parallel to the direction of propagation. We are interested in the solution of the wave equation for the out-of-plane vibrations in the form

$$\nabla^2\phi+k^2\phi=0, \tag{8}$$

where $\phi\equiv u_z$, $k\equiv k_t$, and $\nabla^2\equiv\nabla_p^2$. It is very important to note that we consider, for the sake of simplicity, that the outer medium containing the said acoustic device is made up of some high-density, infinitely rigid material. The resulting situation is equivalent to that attained in the case of similar electronic devices surrounded by infinitely repulsive walls.[8]

In order to solve the scalar equation and describe the system we use the same transfer-matrix method that was employed in the study of electronic[10,8] and photonic[9] tuners. The method relates the incoming to the outgoing wave across the stub for arbitrary initial conditions. Inside the waveguide segments, since the solution must vanish on the walls, the y dependence is $\sin[n\pi(y+c/2)/c]$ for the left segment, for example. Here the integer n defines the number of modes in the respective waveguide. When the two segments connected with the stub have different widths and elastic properties, the respective solutions are given by

$$\phi_1=\sum_m\,[c_{1m}e^{i\beta_m x}+\overline{c}_{1m}e^{-i\beta_m x}]\sin[c_m(y+c/2)] \tag{9}$$

on the left segment and by

$$\phi_2=\sum_n\,[c_{2n}e^{i\alpha_n(x-b)}+\overline{c}_{2n}e^{-i\alpha_n(x-b)}]\sin[a_n(y+a/2)] \tag{10}$$

on the right segment. Here $a_n=n\pi/a$, $c_m=m\pi/c$,

$$\alpha_n=\sqrt{k_1^2-a_n^2},\quad k_1=\omega/v_1, \tag{11}$$

and

$$\beta_m=\sqrt{k_2^2-c_m^2},\quad k_2=\omega/v_2, \tag{12}$$

with $v_1(v_2)$ the transverse speed of sound of the material in the right (left) segment. Inside the stub, ϕ must vanish at $y=d-h/2$ and $y=d+h/2$; thus the basic y dependence is $\sin(k\pi y_\pm/h)$, where $y_\pm=y\mp h/2-d$. However, the internal solution should also vanish at each side of the stub outside the main segments, and smoothly connect to the external one

across the contact boundaries between the stub and the segments (at $x=0$ and $x=b$). We first construct two auxiliary sets of solutions to the wave equation, one of which matches the waveguide on the left and one on the right, with each vanishing elsewhere on the boundary. The appropriate boundary conditions are

$$\chi_{kL}(x=b,y)=0, \tag{13}$$

$$\chi_{kL}(x=0,y)=\begin{cases} 0, & y>c/2, \\ \sin[c_k(y+c/2)], & -c/2<y<c/2, \\ 0, & y<-c/2 \end{cases} \tag{14}$$

and

$$\chi_{kR}(x=0,y)=0, \tag{15}$$

$$\chi_{kR}(x=b,y)=\begin{cases} 0, & y>a/2, \\ \sin[a_k(y+a/2)], & -a/2<y<a/2, \\ 0, & y<-a/2, \end{cases} \tag{16}$$

where the subscript $k(j\equiv L,R)$ refers to the number of modes (left/right segments). The solutions χ_{kR} are expanded as

$$\chi_{kR}=\sum_n [u_n \sin(\gamma_n x)+v_n \cos(\gamma_n x)]\sin(h_n y_-), \tag{17}$$

where

$$y_-=y+h/2-d, \quad h_n=n\pi/h,$$

and

$$\gamma_n=\sqrt{k_s^2-h_n^2}, \quad k_s=\omega/v_s, \tag{18}$$

with v_s the transverse speed of sound of the material in the stub. The boundary condition at $x=0$ requires $v_n=0$, whereas the condition at $x=b$ yields

$$\sum_n u_n \sin(\gamma_n b)\sin(h_n y_-) = \begin{cases} 0, & y>a/2, \\ \sin[a_k(y+a/2)], & -a/2<y<a/2, \\ 0, & y<-a/2. \end{cases} \tag{19}$$

This is a Fourier expansion with the coefficients u_n given by

$$u_m=\frac{2}{h\sin(\gamma_m b)} I_{km}^R, \quad m=1,2,\ldots, \tag{20}$$

where

$$I_{km}^R=\int_{-a/2}^{+a/2} dy \sin[a_k(y+a/2)]\sin(a_m y_-) \tag{21}$$

$$=\frac{a}{2\pi}\left\{\frac{1}{(k-ma/h)}[\sin(k\pi-h_m s_+)+\sin(h_m s_-)] - \frac{1}{(k+ma/h)}[\sin(k\pi+h_m s_+)-\sin(h_m s_-)]\right\} \tag{22}$$

and $s_\pm=h/2\pm a/2-d$; then from Eq. (15) we have

$$\chi_{kR}=\frac{2}{h}\sum_m \frac{\sin(\gamma_m x)}{\sin(\gamma_m b)} I_{km}^R \sin(h_m y_-). \tag{23}$$

Following the same procedure, we find that

$$\chi_{kL}=\frac{2}{h}\sum_m \frac{\sin[\gamma_m(b-x)]}{\sin(\gamma_m b)} I_{km}^L \sin(h_m y_-), \tag{24}$$

where I_{km}^L is defined just as I_{km}^R with a replaced by c. The actual wave function in the stub region can be expanded in terms of these auxiliary solutions χ_{kR} and χ_{kL}

$$\phi_s=\sum_k (f_k\chi_{kL}+\overline{f}_k\chi_{kR}). \tag{25}$$

The continuity of the wave function at $x=0$ and b requires $f_k=c_{1k}+\overline{c}_{1k}$ and $\overline{f}_k=c_{2k}+\overline{c}_{2k}$. Thus one can write

$$\phi_s=\frac{2}{h}\sum_{km}\left[(c_{2k}+\overline{c}_{2k})\frac{\sin(\gamma_m x)}{\sin(\gamma_m b)} I_{km}^R + (c_{1k}+\overline{c}_{1k})\frac{\sin[\gamma_m(b-x)]}{\sin(\gamma_m b)} I_{km}^L\right]\sin(h_m y_-). \tag{26}$$

Similarly, matching the derivative at $x=0$ gives

$$\sum_n (c_{1n}-\overline{c}_{1n}) i\beta_n \sin[c_n(y+c/2)] = \frac{2}{h}\sum_{km}\frac{(c_{2k}+\overline{c}_{2k})I_{km}^R-(c_{1k}+\overline{c}_{1k})\cos(\gamma_m b)I_{km}^L}{\sin(\gamma_m b)} \times \gamma_m \sin(h_m y_-), \tag{27}$$

and at $x=b$,

$$\sum_n (c_{2n}-\overline{c}_{2n}) i\alpha_n \sin[a_n(y+a/2)] = \frac{2}{h}\sum_{km}\frac{(c_{2k}+\overline{c}_{2k})\cos(\gamma_m b)I_{km}^R-(c_{1k}+\overline{c}_{1k})I_{km}^L}{\sin(\gamma_m b)} \times \gamma_m \sin(h_m y_-). \tag{28}$$

Multiplying Eq. (27) by $\sin[c_l(y+c/2)]$ on both sides and integrating from $-c/2$ to $c/2$ gives

$$(c_{1l}-\overline{c}_{1l}) i\beta_l = \frac{4}{ch}\sum_{km}\frac{(c_{2k}+\overline{c}_{2k})I_{km}^R-(c_{1k}+\overline{c}_{1k})\cos(\gamma_m b)I_{km}^L}{\sin(\gamma_m b)} \times \gamma_m I_{lm}^L. \tag{29}$$

Similarly, multiplying Eq. (28) by $\sin[a_l(y+a/2)]$ on both sides and integrating from $-a/2$ to $a/2$ yields

$$(c_{2l}-\overline{c}_{2l})i\alpha_l = \frac{4}{ah}\sum_{km}\frac{(c_{2k}+\overline{c}_{2k})\cos(\gamma_m b)I^R_{km}-(c_{1k}+\overline{c}_{1k})I^L_{km}}{\sin(\gamma_m b)} \times \gamma_m I^R_{lm}. \tag{30}$$

We define

$$c^{\pm}_k = c_k \pm \overline{c}_k \tag{31}$$

to cast Eqs. (29) and (30) in the form

$$i\beta_l c^-_{1l} = \frac{4}{ch}\sum_{km}\frac{\gamma_m I^L_{lm}}{\sin(\gamma_m b)}[c^+_{2k}I^R_{km}-c^+_{1k}\cos(\gamma_m b)I^L_{km}] \tag{32}$$

and

$$i\alpha_l c^-_{2l} = \frac{4}{ah}\sum_{km}\frac{\gamma_m I^R_{lm}}{\sin(\gamma_m b)}[c^+_{2k}\cos(\gamma_m b)I^R_{km}-c^+_{1k}I^L_{km}]. \tag{33}$$

We now define matrices $\hat{A}$, $\hat{B}$, $\hat{D}$, $\hat{E}$, and $\hat{\alpha}$ whose elements are

$$A^{LL}_{lk} = \frac{4}{ch}\sum_m \frac{\cos(\gamma_m b)}{\sin(\gamma_m b)}\gamma_m I^L_{lm}I^L_{km}, \tag{34}$$

$$B^{LR}_{lk} = \frac{4}{ch}\sum_m \frac{1}{\sin(\gamma_m b)}\gamma_m I^L_{lm}I^R_{km}, \tag{35}$$

$$D^{RL}_{lk} = \frac{4}{ah}\sum_m \frac{1}{\sin(\gamma_m b)}\gamma_m I^R_{lm}I^L_{km}, \tag{36}$$

$$E^{RR}_{lk} = \frac{4}{ah}\sum_m \frac{\cos(\gamma_m b)}{\sin(\gamma_m b)}\gamma_m I^R_{lm}I^R_{km}, \tag{37}$$

$$\alpha_{lk} = i\alpha_l\delta_{lk}, \quad \beta_{lk} = i\beta_l\delta_{lk}. \tag{38}$$

We also define the column vectors C^+_i and C^-_i whose elements are c^+_{ik} and c^-_{ik}, respectively. In this notation, we have

$$\hat{\beta}C^-_1 = -\hat{A}C^+_1 + \hat{B}C^+_2, \tag{39}$$

$$\hat{\alpha}C^-_2 = -\hat{D}C^+_1 + \hat{E}C^+_2, \tag{40}$$

where $\hat{A}$, $\hat{B}$, $\hat{D}$, and $\hat{E}$ are real-valued matrices. These two equations determine C^+_1 and C^-_1 in terms of C^+_2 and C^-_2. The result is

$$\begin{pmatrix} C^+_1 \\ C^-_1 \end{pmatrix} = \hat{M}^{\beta\alpha}\begin{pmatrix} C^+_2 \\ C^-_2 \end{pmatrix}, \tag{41}$$

where $\hat{M}^{\beta\alpha}$ is the resulting transfer matrix with matrix elements

$$M^{\beta\alpha}_{11} = \hat{D}^{-1}\hat{E}, \quad M^{\beta\alpha}_{12} = -\hat{D}^{-1}\hat{\alpha}, \tag{42}$$

$$M^{\beta\alpha}_{21} = -\hat{\beta}^{-1}\hat{A}\hat{D}^{-1}\hat{E} + \hat{\beta}^{-1}\hat{B}, \quad M^{\beta\alpha}_{22} = \hat{\beta}^{-1}\hat{A}\hat{D}^{-1}\hat{\alpha}. \tag{43}$$

This transfer matrix relates the incoming to the outgoing wave across the stub for arbitrary initial conditions.

The other building block of a multiple-stub system is a stubless waveguide segment. The transfer matrix induced by the segment of length l_{ij} connecting the ith and jth stub is a special case of the matrix $\hat{M}^{\beta\alpha}$ in Eq. (41). This is obtained by considering the special case $c=a=h$, $d=0$, $\alpha_n=\beta_n$, and $k_2=k_1=k_s$. The result is

$$\hat{P}_{(ij)} = \begin{bmatrix} \cos(\alpha l_{ij}) & -i\sin(\alpha l_{ij}) \\ -i\sin(\alpha l_{ij}) & \cos(\alpha l_{ij}) \end{bmatrix}, \tag{44}$$

where $j=i\pm 1$. Given $\hat{M}^{\beta\alpha}$ and $\hat{P}$, the total transfer matrix for an n-stub system is

$$\hat{M}^T = \prod_{i=1}^{n-1}[\hat{M}^{\beta\alpha}(i)\hat{P}(i,i+1)]\hat{M}^{\beta\alpha}(n). \tag{45}$$

Suppose the incident wave, at the entrance of the first stub, is represented by $\{C^+_{\rm in}, C^-_{\rm in}\}$ and the outgoing one, at the exit of the last stub, by $\{C^+_{\rm out}, C^-_{\rm out}\}$. Then

$$\begin{pmatrix} C^+_{\rm in} \\ C^-_{\rm in} \end{pmatrix} = \hat{M}^T\begin{pmatrix} C^+_{\rm out} \\ C^-_{\rm out} \end{pmatrix}. \tag{46}$$

We now discuss the physical conditions imposed on the incoming and outgoing wave components. Depending on the frequency, α_n and β_n could be real or pure imaginary. We choose them to be positive for an open channel and lying on the positive imaginary axis for a closed channel, so a complete set of eigenfunctions of Eq. (8) is obtained. With this choice, $\overline{C}_{{\rm out},n}$ represents either a leftward moving wave or an exponentially divergent wave at positive infinity. Now, for the sake of the argument, we will take the incident wave to come from the left; in this situation, we must set $\overline{C}_{\rm out}=0$ and thus $C^+_{\rm out}=C^-_{\rm out}=C_{\rm out}$. Physically $c_{{\rm out},n}$ represents the transmitted wave components in the nth mode. In the entrance region the components $\overline{c}_{{\rm in},n}$ are allowed. Here $\overline{c}_{{\rm in},n}$ represents the amplitude of the reflected wave in the nth mode in the open channel. For a closed channel the reflected wave is a transient and decays exponentially. Explicitly,

$$C^+_{\rm in} = C_{\rm in} + \overline{C}_{\rm in} = \hat{M}^T_{11}C_{\rm out} + \hat{M}^T_{12}C_{\rm out}, \tag{47}$$

$$C^-_{\rm in} = C_{\rm in} - \overline{C}_{\rm in} = \hat{M}^T_{21}C_{\rm out} + \hat{M}^T_{22}C_{\rm out}, \tag{48}$$

where $\hat{M}^T_{ij}$ are blockwise submatrices of $\hat{M}^T$. Adding these two equations we can determine the transmitted amplitudes $C_{\rm out}$ by solving

$$2C_{\rm in} = \left(\sum_{ij}\hat{M}^T_{ij}\right)C_{\rm out}. \tag{49}$$

Following this, the reflection coefficients are given by

$$\overline{C}_{\rm in}=\frac{1}{2}(\hat{M}_{11}^{T}+\hat{M}_{12}^{T}-\hat{M}_{21}^{T}-\hat{M}_{22}^{T})C_{\rm out}. \tag{50}$$

The total transmission and reflection coefficients are then given by

$$T=\frac{\Sigma_{n\epsilon\{\rm open\}}c_{{\rm out},n}c^{*}_{{\rm out},n}\alpha_n}{\Sigma_{n\in\{\rm open\}}c_{{\rm in},n}c^{*}_{{\rm in},n}\alpha_n} \tag{51}$$

and

$$R=\frac{\Sigma_{n\in\{\rm open\}}\overline{c}_{{\rm in},n}\overline{c}^{*}_{{\rm in},n}\alpha_n}{\Sigma_{n\in\{\rm open\}}c_{{\rm in},n}c^{*}_{{\rm in},n}\alpha_n}. \tag{52}$$

For the sake of completeness, it is noteworthy that for the bound-state calculation, one must solve the homogeneous version of Eq. (49).

We also stress that in this formalism, once we know how to handle the single stub case, the multiple-stub problem can be dealt with little additional labor. This is not the case with either the recursive Green-function method or the usual mode-matching approach.

Finally, the band structure for a periodic system of acoustic stub tuners is computed by solving the standard eigenvalue equation

$$\hat{M}^{B}\Phi=e^{ik_xL}\hat{I}\Phi, \tag{53}$$

where k_x is the Bloch vector and $L=b+l$ is the period of the 1D superlattice of acoustic stub tuners. The matrix $\hat{M}^{B}$ is the same as $\hat{M}^{T}$ for the unit cell but with $c=a$ and $\beta_n=\alpha_n$, $\hat{I}$ is the unit matrix of the same order as $\hat{M}^{B}$, and Φ is the column eigenvector. So the strategy of the computation is that we input the dimensionless frequency $\Omega=\omega L/\pi v_{wg}$ and calculate $w=\exp(ik_xL)$, yielding $k_x=-(i/L)\ln(w)$. For $|w|=1$ $(\neq 1)$ one obtains bands (gaps) in the band structure for a given set of material and geometrical parameters. It should be pointed out that in order to make this paper as self-consistent as possible we have heavily relied on Ref. 10 in this section.

III. ILLUSTRATIVE EXAMPLES

For the sake of clarity we discuss the numerical results in two parts. First, we consider the case when the waveguide and the stubs are made up of the same material. Clearly the band structure and/or transmission spectrum in this case reveals the influence of the various parameters involved in the problem. Then we take up the case when the materials in the waveguide and the stubs are different. Practically speaking, this case is more complex but richer than the previous one in the sense that one has more options to modulate the band structure and/or transmission spectrum. We have chosen carbon and epoxy resin as the suitable materials the acoustic system considered is made of. This is because these are the materials whose combination was first demonstrated to give rise to a complete band gaps, i.e., independent of the polarization of the wave and of the direction of propagation, in 2D periodic phononic crystals.[13] The parameters used are ρ $=1.75$ (1.2) g/cm^3 and $v_t=711{,}095$ (115,830) cm/sec for carbon (epoxy).

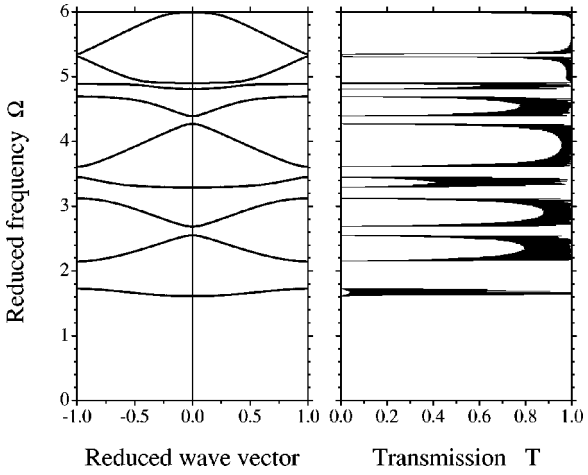

FIG. 3. Band structure (left panel) and transmission spectrum (right panel) for a system with the same material, epoxy, in the waveguide and the stubs. The reduced wave vector and frequency are defined by k_xL/π and $\Omega=L\Omega/\pi v_1$, where v_1 is the transverse speed of sound in the waveguide. Notice the lowest acoustic gap below the cutoff frequency $\Omega_c\simeq 1.6$. For the plot of the transmission a system of fifty ($n=50$) stubs was considered.

A. Same material in waveguide and stubs

The left part of Fig. 3 shows the first nine bands for a symmetrically stubbed system made up of epoxy, with parameters $a_L=a/L=0.5114$, $b_L=b/L=0.4886$, $h_L=h/L=1.125$, and $d_L=d/L=0.0$. As one can see, all the nine bands are separated from each other by stop bands, or gaps, within which the acoustic wave propagation is forbidden. Unlike the other 2D and 3D periodic systems,[2,4] there is a complete gap below a cutoff frequency $\Omega_c\simeq 1.6$ down to $\Omega=0$. It is found that this (the lowest) gap persists independent of the values of the variable parameters. The existence of all nine gaps is well corroborated by the energy dependence of the transmission coefficient for $n_{\rm stub}=50$ on the right part of Fig. 3. The numerical results clearly reveal the zeros and ones in the transmission. It is noteworthy that the band structure in this figure contains both direct and indirect gaps. For instance, the second, third, fifth, sixth, and ninth gaps are direct, while the rest are indirect. We consider it more appropriate to include the lowest (and also the widest) gap in the category of direct gaps. The most important aspect of these results is the cutoff frequency Ω_c below which no propagation at all is allowed.

Figure 4 depicts the dimensionless gap widths of the three lowest gaps of Fig. 3 as a function of the dimensionless stub width b_L and the stubs are symmetric, i.e., $d=0$. The width of the lowest gap Δ_1 decreases gradually, by approximately 45%, with increasing b_L but still remains finite for $b\rightarrow L$. We notice that the maximum of Δ_1 is near the cutoff frequency of the waveguide segments $\Delta_w=1/a_L=1.96$ and the minimum of Δ_1 is near the cutoff frequency of the stub segments $\Delta_s=1/h_L=0.89$. In general, the cutoff frequency of the com-

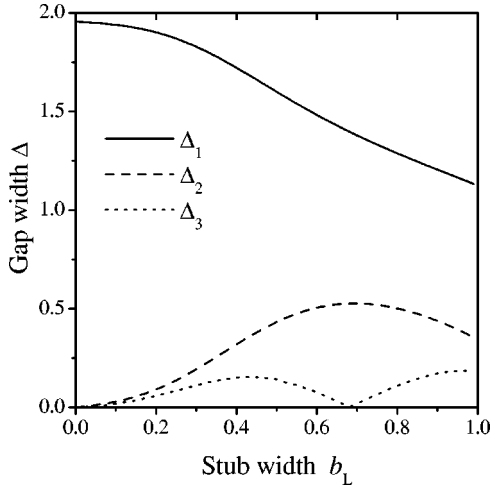

FIG. 4. The widths of the three lowest gaps as a function of the stub width $b_L = b/L$. The solid, dashed, and dotted curves refer to the lowest (Δ_1), second lowest (Δ_2), and third lowest (Δ_3) gaps. The material and the rest of the parameters are the same as those in Fig. 3.

bined system is between the one of the waveguide segments and that for the stub segments. The second lowest gap Δ_2 reaches a maximum for $b_L \simeq 0.7$ and decreases slightly before approaching the final minimum at $b \to L$. As can be seen, this gap increases enormously relative to its value for zero stub width. Similarly, the third lowest gap Δ_3 reaches one maximum at $b_L \simeq 0.44$, it then vanishes at $b_L \simeq 0.68$, and finally reaches a maximum at $b_L \to 1$. Note that all three gaps start opening up at a vanishingly small but finite value of b_L and that the lowest gap remains the widest one over the whole range of the stub width.

Figure 5 represents the band structure and the corresponding transmission spectrum for asymmetric stubs, with d

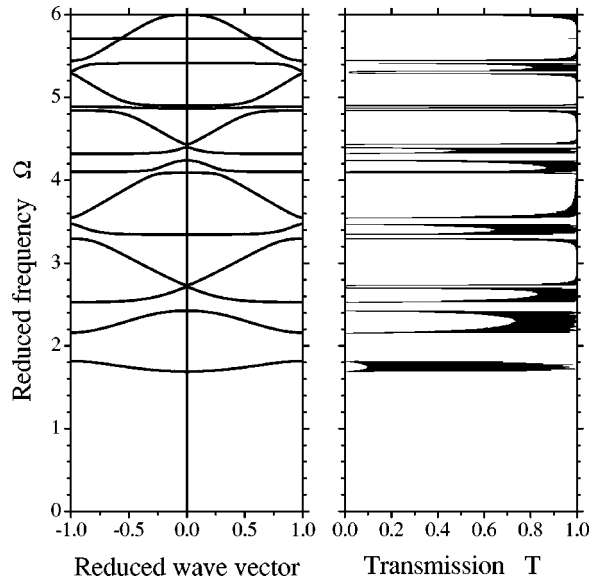

FIG. 5. Same as in Fig. 3, but for asymmetric stubs with asymmetry parameter $d_L = 0.25$. Notice the lowest acoustic gap below the cutoff frequency $\Omega_c \simeq 1.7$.

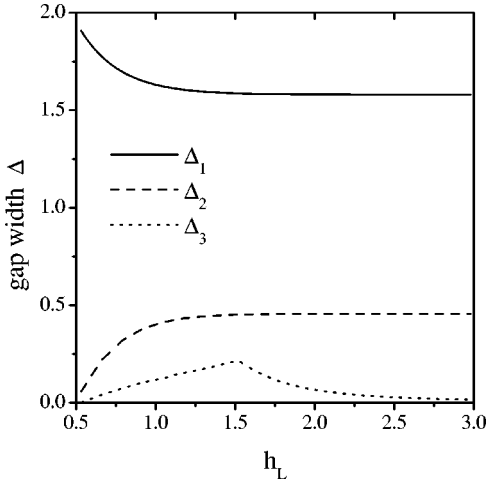

FIG. 6. The widths of the three lowest gaps as a function of the stub length $h_L = h/L$. The curves are marked as in Fig. 4.

$= 0.25$. The rest of the parameters are the same as in Fig. 3. We observe that the asymmetry has introduced two important effects. First, the number of bands accommodated within the same frequency range has increased, from 9 to 14. Second, the band width of most of the bands has reduced. Overall, the effect of the asymmetry seems to result in gaps larger in number but shorter in width. This is true despite some exceptions, for instance, the case of the lowest gap, which now extends from $\Omega = 0$ to $\simeq 1.7$, instead of up to $\Omega \simeq 1.61$ in Fig. 3. All gaps in the band structure (left part of Fig. 5) are seen to be well substantiated by those in the transmission spectrum (right part of Fig. 5) for $n = 50$.

As a function of the asymmetry parameter d the three lowest gaps vary very little, by at most 10%, for $0 \leqslant d \leqslant 0.3$. Their dependence on b_L is similar to that shown in Fig. 4. As a function of the stub length h_L their behavior, shown in Fig. 6, is similar to that in Fig. 4 for Δ_1 and Δ_2 but

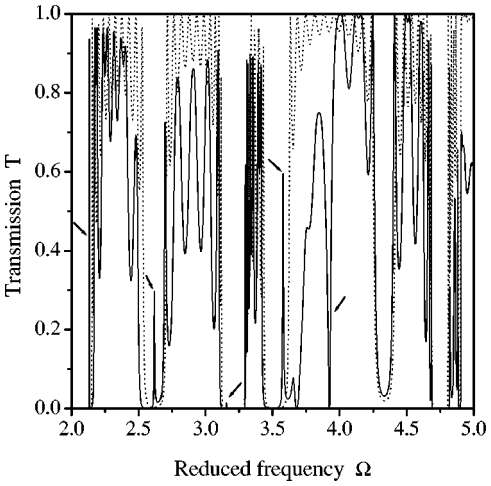

FIG. 7. Transmission spectrum for a system with eleven symmetric double stubs ($n = 11$). The central (sixth) symmetric stub is a defect with $h_L = 1.395$ and $b_L = 0.6305$. The rest of the parameters are the same as in the previous figures. Notice that the defect creates new modes or states in the gaps in an otherwise defect-free system. The peaks of these modes are marked with arrows.

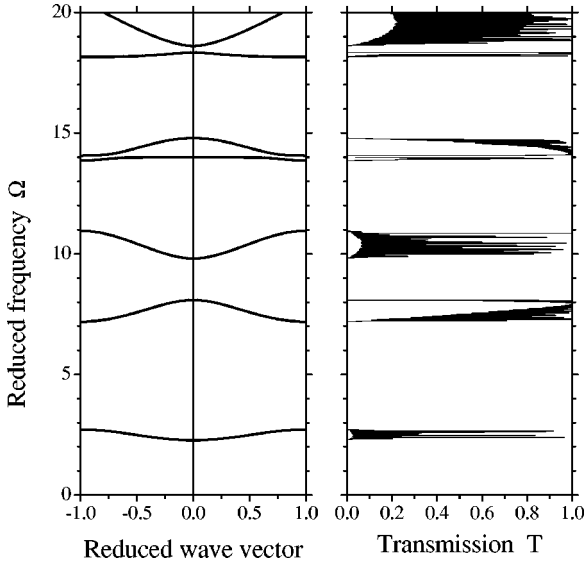

FIG. 8. Band structure (left panel) and transmission spectrum (right panel) for system with symmetric stubs with the waveguide segments (stubs) made of epoxy (carbon). The parameters used are $a_L=0.9$, $b_L=0.9$, and $h_L=1.5$. Notice the lowest acoustic gap below the cutoff frequency $\Omega_c\simeq 2.3$ and extending down to $\Omega=0.0$.

somewhat different for Δ_3.

Figure 7 shows the transmission spectrum versus reduced frequency for a system made up of eleven symmetric stubs with the central (sixth) stub longer ($h_L=1.395$) and wider ($b_L=0.6305$) than the rest of the identical, in width and height, stubs. When not identical to the other stubs, this central stub constitutes a defect. The solid (dotted) curves correspond to the presence (absence) of this defect. One can see that there are five complete gaps in the spectrum within the given frequency range. In addition, there is also a pseudogap, centered at $\Omega\simeq 4.35$, that corresponds to the low transmission or density of states. The defect introduces sharp transmission peaks, marked by arrows, within the first four gaps in plane analogy with the electronic[8] and photonic[9] case or with that of surface modes of a truncated superlattice.[14] Another interesting consequence of introducing a defect in the system is the appearance of antiresonances,[9] such as the one appearing in the fourth band at $\Omega\simeq 3.92$. We have noted similar effects in the case of an asymmetric ($d\neq 0$) defect introduced in the system.

B. Different materials in waveguide and stubs

We now present numerical results for a system in which the waveguide is made of epoxy and the stubs of carbon. Figure 8 shows the band structure and transmission spectrum for symmetric stubs; the parameters are $a_L=0.9$, $b_L=0.9$, $h_L=1.5$, and $d_L=0.0$. We note that there are only seven bands accommodated in the frequency range $0\leqslant\Omega\leqslant 20$, and every pair of bands has a full gap in between. Moreover, the lowest acoustic gap extends from zero to the cutoff frequency $\Omega_c\simeq 2.3$. Some of the bands, such as the fourth and sixth, are seen to be almost flat and hence have vanishingly small group velocity. All gaps in the band structure (left panel) correspond well to those in the transmission spectrum for $n=50$ on the right panel. A prompt comparison of Figs. 8 and 3 reveals that one can achieve wider gaps in the band structure if the segments and stubs are made up of different materials.

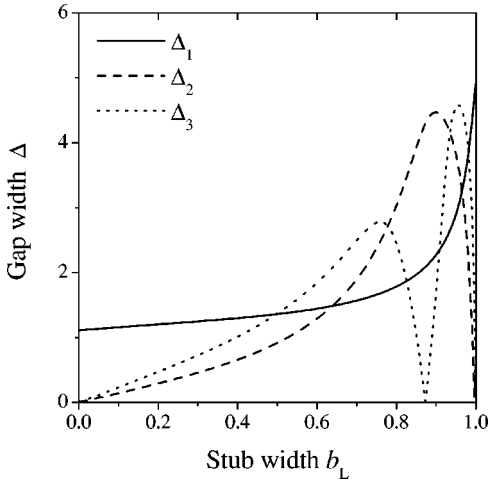

FIG. 9. The widths of the three lowest gaps versus the stub width b_L for the system studied in Fig. 8. The solid, dashed, and dotted lines refer, respectively, to the lowest (Δ_1), second lowest (Δ_2), and third lowest (Δ_3) gaps. Notice especially the strong variation of Δ_2 and Δ_3.

Figure 9 shows the three lowest gaps as a function of the stub width b_L for the system specified in Fig. 8. There are several noteworthy points. First, the lowest gap is the widest one and the third gap is wider than the second one until $b_L\simeq 0.49$, where $\Delta_1=\Delta_3$. At $b_L\simeq 0.64$, the width of the lowest and second lowest gaps are equal, i.e., $\Delta_1=\Delta_2$. Also $\Delta_2=\Delta_3$ at $b_L\simeq 0.78$ and 0.94. The second lowest gap is the widest one in the range specified by $0.78\leqslant b_L\leqslant 0.94$. The

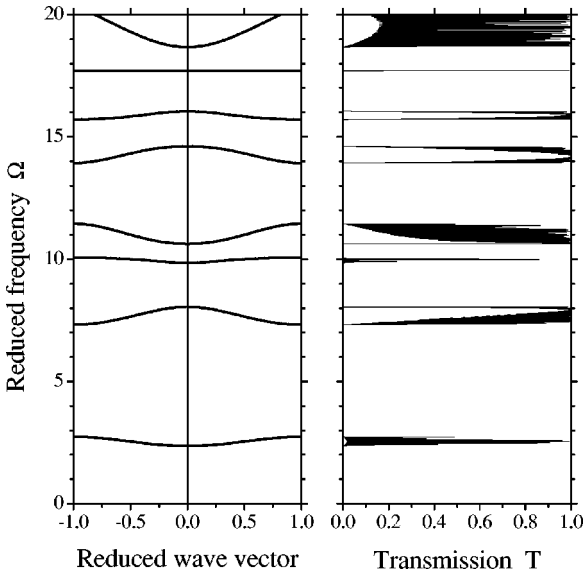

FIG. 10. Same as in Fig. 8, but for a system with asymmetric stubs ($d_L=0.25$). The lowest acoustic gap occurs below the cutoff frequency $\Omega_c\simeq 2.4$ and down to $\Omega=0.0$.

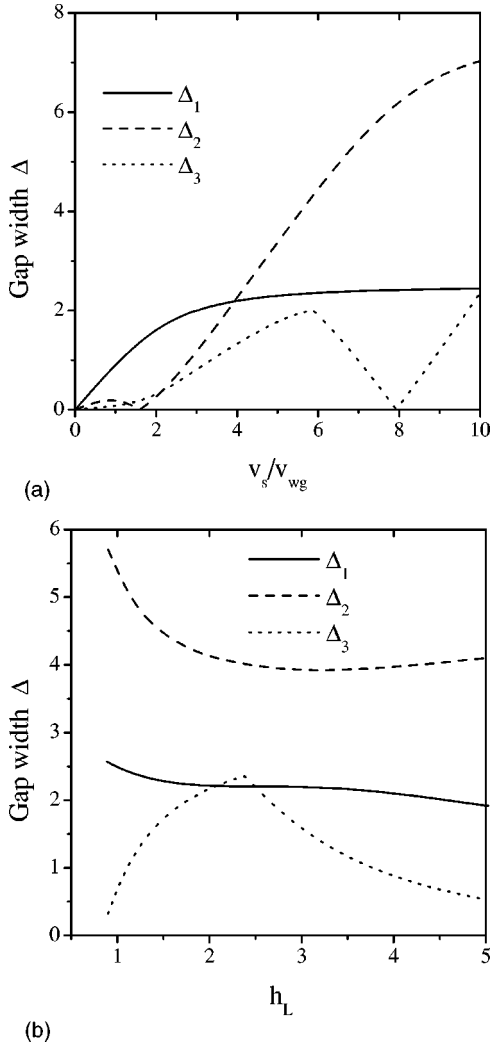

FIG. 11. (a) The widths of the three lowest gaps as a function of the velocities' ratio v_s/v_{wg}. (b) The three lowest gaps as a function of the stub length h_L. Notice the strong variation of Δ_2 and Δ_3, especially in (a).

third lowest gap vanishes at $b_L \simeq 0.87$ but reappears for $b_L > 0.87$ and becomes the widest in the range $0.94 \leqslant b_L \leqslant 0.98$. Also, $\Delta_1 = \Delta_3$ at $b_l \simeq 0.83$ and 0.91. Moreover, $\Delta_1 = \Delta_2$ at $b_L \simeq 0.96$ and $\Delta_1 = \Delta_3$ at $b_L \simeq 0.98$. Finally, Δ_1 reaches a maximum whereas both Δ_2 and Δ_3 vanish for $b \rightarrow L$. Similar to Fig. 4, the minimum of Δ_1 here is near the cutoff frequency of the waveguide segments $\Delta_w = 1/a_L = 1.1$ and the maximum of Δ_1 is near the cutoff frequency of the stub segments $\Delta_s = v_s/(v_1 h_L) = 4.1$. Again the cutoff frequency of the combined system is between the one of the waveguide segments and that for the stub segments. The relative position though depends on b_L and the velocity contrast and can be outside the range (Δ_w, Δ_s).

Figure 10 depicts the band structure and transmission spectrum considered in Fig. 8 but with asymmetric stubs. The asymmetry parameter is $d_L = 0.25$ and the other parameters the same as those used in Fig. 8. Now there are eight bands and eight gaps in the band structure. The lowest gap now extends from $\Omega = 0.0$ to $\Omega \simeq 2.4$. The asymmetry is seen

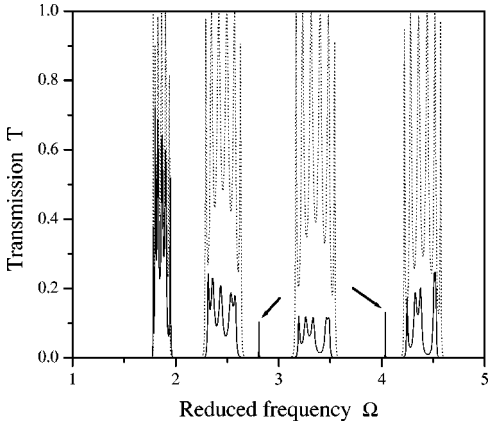

FIG. 12. Transmission spectrum for a system with seven symmetric ($d = 0$) double stubs ($n = 7$). The waveguide segments (stubs) are made of epoxy (carbon). The central (fourth) stub is a defect with $h_L = 3.0$ and $b_L = 0.4$. The other parameters are $a_L = 0.6$, $b_L = 0.2$, and $h_L = 1.4$. The solid (dotted) lines refer to the transmission with (without) the defect. The defect gives rise to modes in the gaps in an otherwise defect-free system. The peaks of these modes are marked with arrows.

to have brought about a number of interesting effects. A larger number of bands is accommodated in the same frequency range but the bandwidth is reduced. Again, the gaps in the band structure (left panel) correspond well to those in the transmission spectrum for a system with $n = 50$ stubs (right panel).

As a function of the stub width b_L the three lowest gaps behave qualitatively as those of Fig. 9. More important is their dependence, shown in Fig. 11(a), on the velocity contrast between two materials. As can be seen a wide modulation can be achieved in this asymmetric structure by just changing the ratio v_g/v_{wg}, more than two orders of magnitude for Δ_2. A less pronounced variation of the same gaps is shown in Fig. 11(b) as a function of the stub length h_L. As can be seen, Δ_1 remains almost insensitive to changes in h_L and Δ_2 changes by at most 30%; however, Δ_3 can change by a factor of 10 reaching a maximum at $h_L \sim 2.4$.

Figure 12 shows the transmission spectrum versus reduced frequency for a symmetric defect introduced in an otherwise periodic system with seven stubs ($n = 7$). The central (fourth) stub is defect in the sense that its length ($h_L = 3.0$) and width ($b_L = 0.4$) are different than those of the rest of the stubs. The other parameters are $a_L = 0.6$, $b_L = 0.2$, $h_L = 1.4$, and $d_L = 0.0$. The solid and dotted curves correspond, respectively, to the presence (absence) of the defect. There are five complete gaps in this frequency range in the spectrum before introducing the defect. Inserting this single defect in the system gives rise to one peak in the third gap and another in the fourth gap. These transmission peaks correspond to defect modes similar to those appearing in Fig. 7.

Finally, Fig. 13 illustrates the transmission spectrum versus reduced frequency Ω in a symmetric system made up of one (top panel), two (middle panel), and five (bottom panel) stubs. We remind the reader that the waveguide segments (stubs) are made of epoxy (carbon) materials. The param-

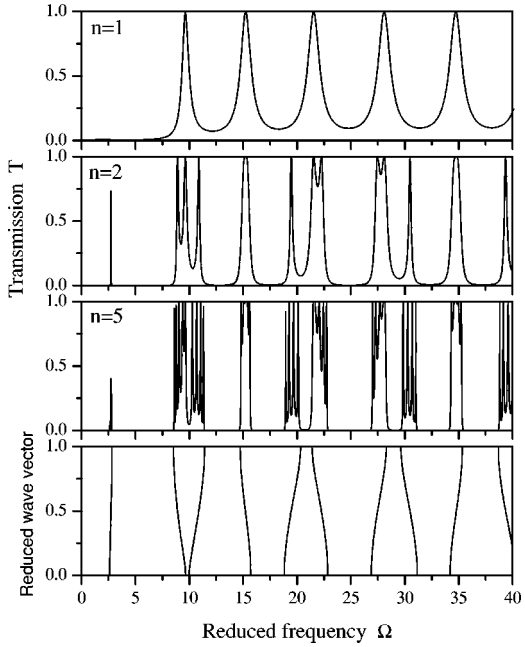

FIG. 13. Evolution of the transmission spectrum as a function of the number of stubs n for a system with waveguide segments (stubs) made of epoxy (carbon). The parameters are $a_L=b_L=h_L=0.9$. Notice that as n increases the pseudogaps gradually turn into sharply defined complete gaps. The lowest panel shows the band structure. Notice that the first band is very narrow.

eters are $a_L=b_L=h_L=0.9$. That is, the waveguide has no stubs. The lowest panel shows the corresponding band structure. For $n=1$ (top panel), the transmission coefficient becomes very small but it never approaches zero. In this sense we have only pseudogaps, not full gaps, in the system. As n increases the pseudogaps gradually turn into complete gaps (with transmission equal to zero) centered at almost the same midgap frequency. It has also been observed that the number of such complete gaps increases with increasing n.

IV. CONCLUDING REMARKS

We have investigated the existence of tunability of complete spectral gaps in the band structure of a quasi-one-dimensional waveguide with double stubs periodically grafted at N equidistant sites. The waveguide segments and the stubs can be made up of same or different materials. The latter case is found to be relatively more interesting since there one has more and better options to achieve the complete gaps. The single symmetric defect is shown to introduce extra modes in the gaps of an otherwise periodic system that result in transmission resonance peaks. While the computation of the band structure requires an infinitely long periodic system, the transmission spectrum is calculated only for a finite system. As shown though, the gaps in the band structure correspond well to those in the transmission spectrum. Accordingly, we conclude that the transmission spectrum in all cases remains consistent for $n \geqslant 10$.

The numerical results we presented pertain only to the out-of-plane modes. However, as mentioned already in Sec. II A, the equations describing the in-plane modes have the same structure in a homogeneous medium. Explicitly, the transverse in-plane modes have exactly the same band structure as the out-of-plane modes. As for the longitudinal in-plane modes, their band structure and transmission can be obtained directly from Figs. 3–7 by changing only the frequency scale when the waveguide and the stubs are made of the same material. If this material is different, the separation of the in-plane modes in longitudinal and transverse is no longer possible for the structures of Sec. III B (see Sec. II A).

The version of the transfer-matrix method employed[10] to accomplish the present investigation is simple and efficient[8–10] for solving scalar equations. Its efficiency has already been demonstrated in serially connected electronic,[8,10] optical,[9] or the present acoustic devices. As stressed already in its presentation, the method offers important advantages in comparison to other mode-matching or recursive Green's function techniques applied to similar problems.

In principle, the systems we studied here have potential applications in the designing of transducers and ultrasonic filters. We hope that the present findings will be tested in future experiments.

ACKNOWLEDGMENTS

This work was supported by the NSERC Grant No. OGP0121756. The work of M. S. K. was also supported by CONACyT Grant No. 28110-E.

[1] *Photonic Band Gap Materials*, edited by C. M. Soukoulis (Kluwer, Dortrecht, 1996).

[2] M. S. Kushwaha, P. Halevi, L. Dobrzynski, and B. Djafari-Rouhani, Phys. Rev. Lett. **71**, 2022 (1993); **75**, 3581 (1995).

[3] M. M. Sigalas and E. N. Economou, Europhys. Lett. **36**, 241 (1996); M. Kafesaki and E. N. Economou, Phys. Rev. B **60**, 11 993 (1999); C. E. Bradley, J. Acoust. Soc. Am. **96**, 1844 (1994); J. De Poorter and D. Botteldooren, *ibid.* **104**, 1171 (1998); C. Depolier, J. Kergomard, and J. C. Lesueur, J. Sound Vib. **142**, 153 (1990).

[4] M. S. Kushwaha, Appl. Phys. Lett. **70**, 3218 (1997).

[5] F. R. Montero de Espinoza, E. Jimenez, and M. Torres, Phys. Rev. Lett. **80**, 1208 (1998); J. V. Sánchez-Pérez, D. Caballero, R. Mártinez-Sala, J. Sánchez-Dehesa, F. Meseguer, J. Llinares, and F. Gálvez, *ibid.* **80**, 5325 (1998); D. García-Pablo, M. Sigalas, F. R. Montero-Espinosa, M. Torres, M. Kafesaki, and N. García, *ibid.* **84**, 4349 (2000).

[6] W. M. Robertson and J. F. Rudy III, J. Acoust. Soc. Am. **104**, 694 (1998).

[7] R. L. Weaver, Phys. Rev. B **47**, 1077 (1993).

[8] R. Akis, P. Vasilopoulos, and P. Debray, Phys. Rev. B **52**, 2805 (1995); **56**, 9594 (1997).

[9] R. Akis and P. Vasilopoulos, Phys. Rev. E **53**, 5369 (1996).
[10] H. Wu, D. W. L. Sprung, J. Martorell, and S. Klarsfeld, Phys. Rev. B **44**, 6351 (1991).
[11] M. S. Kushwaha, A. Akjouj, B. Djafari-Rouhani, L. Dobrzynski, and J. O. Vasseur, Solid State Commun. **106**, 659 (1998).
[12] L. D. Landau and E. M. Lifshitz, *Theory of Elasticity*, 3rd ed. (Pergamon, Oxford, 1986).
[13] J. O. Vasseur, B. Djafari-Rouhani, L. Dobrzynski, M. S. Kushwaha, and P. Halevi, J. Phys.: Condens. Matter **6**, 8759 (1994).
[14] See, e.g., M. S. Kushwaha, Surf. Sci. Rep. **41**, 1 (2001).